



Eder W.¹, Briguglio A.², Hohenegger J.¹
¹Department of Palaeontology, University of Vienna, Althanstraße 14, 1090 Vienna, Austria, wolfgang.eder@univie.ac.at
²Natural History Museum Vienna, Burgring 7, 1010 Vienna, Austria

It has been identified quite recently that shell form and size of larger benthic foraminifera (LBF) reflect environmental changes. Each growth step of these cells is represented by the addition of a single chamber, or a set of chamberlets. Volume, size and shape of these growth steps are influenced by the environmental scenario the cell is living in. Therefore recent LBF can be used to reconstruct controlling factors that operate as underlying principles to chamber formation. Patterns oscillating around a fixed growth function can be established, which may reflect periodically recurring ecological signals in nature, such as tides, moon cycles or seasonality.

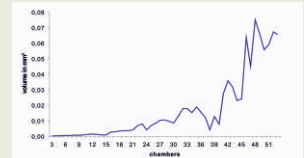


Fig. 1 chamber volume sequence in *H. depressa*.

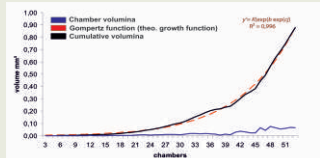


Fig. 2 cumulative volumina and the theoretical growth function (Gompertz function), j = chamber number

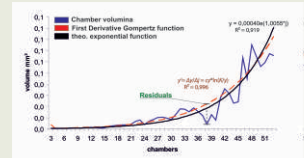


Fig. 3 the chamber volume sequence oscillates around the Gompertz function. The residuals are its deviation from the Gompertz function.

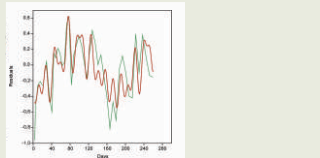


Fig. 4. Residuals are plotted against the day of chamber formation and scanned for periodic cyclicities by using a sinusoidal regression model.

An additional task of this work has been the comparison of growth styles of naturally grown specimens and those cultivated under laboratory conditions, by Röttger and Krüger in 1991. These cyclicities have been calculated and plotted (see Fig. 1-4) in the larger benthic foraminifer, *Heterostegina depressa* using MicroCT technology for volumetry (see Fig. 5-7). Therefore it was a first-hand opportunity to look not only into naturally grown individuals but also cultured specimens of *H. depressa* (see Tab. 1).

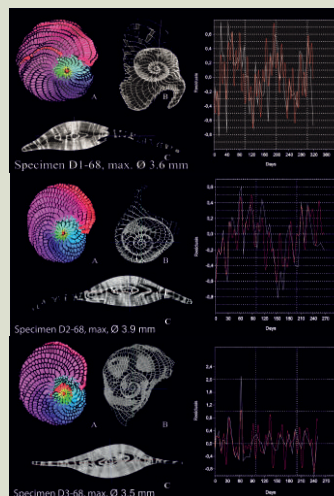


Fig. 5 rendered 3D segmentation (A), equatorial (B) and axial slices (C), as well as sinusoidal function of hawaiian gamonts.

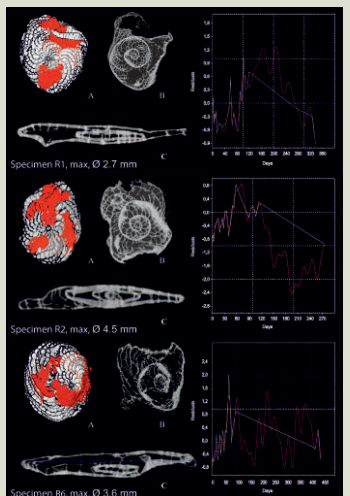


Fig. 6 rendered 3D segmentation (A), equatorial (B) and axial slices (C), as well as sinusoidal function of cultured gamonts. The septal alteration is clearly visible on the radiographs.

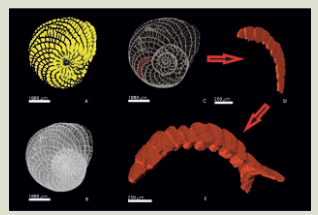


Fig. 7 depicting a 3D segmentation (A), a surface reconstruction (B), a radiographic slice (C). By summing up 2D materials (D) 3D models are gained (E).

Cat.	Origin	Sample No.	Age	Depth in m	Gompertz parameter	Amplitude	Phase	Period	R²
D1-68	Maui, Kekaia Point	888	A	40	$y = 0.0006(1 + 0.0007)^x$ $R^2 = 0.996$	$0.0006(1 + 0.0007)^x$	0.0007	1.00	
D2-68	Maui, Kekaia Point	889	A	40	$y = 0.0006(1 + 0.0007)^x$ $R^2 = 0.996$	$0.0006(1 + 0.0007)^x$	0.0007	1.00	
D3-68	Maui, Kekaia Point	890	A	40	$y = 0.0006(1 + 0.0007)^x$ $R^2 = 0.996$	$0.0006(1 + 0.0007)^x$	0.0007	1.00	
D4-68	Maui, Kekaia Point	891	A	40	$y = 0.0006(1 + 0.0007)^x$ $R^2 = 0.996$	$0.0006(1 + 0.0007)^x$	0.0007	1.00	
R1	Maui, Kekaia Point	P.1.1001	B	n.a.	$y = 0.0006(1 + 0.0007)^x$ $R^2 = 0.996$	$0.0006(1 + 0.0007)^x$	0.0007	1.00	
R2	Maui, Kekaia Point	P.1.1002	B	n.a.	$y = 0.0006(1 + 0.0007)^x$ $R^2 = 0.996$	$0.0006(1 + 0.0007)^x$	0.0007	1.00	
R3	Maui, Kekaia Point	P.1.1003	B	n.a.	$y = 0.0006(1 + 0.0007)^x$ $R^2 = 0.996$	$0.0006(1 + 0.0007)^x$	0.0007	1.00	
R4	Maui, Kekaia Point	P.1.1004	B	n.a.	$y = 0.0006(1 + 0.0007)^x$ $R^2 = 0.996$	$0.0006(1 + 0.0007)^x$	0.0007	1.00	
R5	Maui, Kekaia Point	P.1.1005	B	n.a.	$y = 0.0006(1 + 0.0007)^x$ $R^2 = 0.996$	$0.0006(1 + 0.0007)^x$	0.0007	1.00	
R6	Maui, Kekaia Point	P.1.1006	B	n.a.	$y = 0.0006(1 + 0.0007)^x$ $R^2 = 0.996$	$0.0006(1 + 0.0007)^x$	0.0007	1.00	
A1	Sesoko-Jima	Tanaka A	A	20	$y = 0.0006(1 + 0.0007)^x$ $R^2 = 0.996$	$0.0006(1 + 0.0007)^x$	0.0007	1.00	
A2	Sesoko-Jima	Tanaka A	B	20	$y = 0.0006(1 + 0.0007)^x$ $R^2 = 0.996$	$0.0006(1 + 0.0007)^x$	0.0007	1.00	
A3	Sesoko-Jima	Tanaka A	C	20	$y = 0.0006(1 + 0.0007)^x$ $R^2 = 0.996$	$0.0006(1 + 0.0007)^x$	0.0007	1.00	
A4	Sesoko-Jima	Tanaka A	D	20	$y = 0.0006(1 + 0.0007)^x$ $R^2 = 0.996$	$0.0006(1 + 0.0007)^x$	0.0007	1.00	
A5	Sesoko-Jima	Tanaka A	E	20	$y = 0.0006(1 + 0.0007)^x$ $R^2 = 0.996$	$0.0006(1 + 0.0007)^x$	0.0007	1.00	
B1	Sesoko-Jima	Tanaka B	A	20	$y = 0.0006(1 + 0.0007)^x$ $R^2 = 0.996$	$0.0006(1 + 0.0007)^x$	0.0007	1.00	
B2	Sesoko-Jima	Tanaka B	B	20	$y = 0.0006(1 + 0.0007)^x$ $R^2 = 0.996$	$0.0006(1 + 0.0007)^x$	0.0007	1.00	
B3	Sesoko-Jima	Tanaka B	C	20	$y = 0.0006(1 + 0.0007)^x$ $R^2 = 0.996$	$0.0006(1 + 0.0007)^x$	0.0007	1.00	
B4	Sesoko-Jima	Tanaka B	D	20	$y = 0.0006(1 + 0.0007)^x$ $R^2 = 0.996$	$0.0006(1 + 0.0007)^x$	0.0007	1.00	
B5	Sesoko-Jima	Tanaka B	E	20	$y = 0.0006(1 + 0.0007)^x$ $R^2 = 0.996$	$0.0006(1 + 0.0007)^x$	0.0007	1.00	
C1	Utsunohira	Kiel	F1.27.1.92	A	n.a.	$y = 0.0006(1 + 0.0007)^x$ $R^2 = 0.996$	0.0007	1.00	
C2	Utsunohira	Kiel	F1.27.1.93	A	n.a.	$y = 0.0006(1 + 0.0007)^x$ $R^2 = 0.996$	0.0007	1.00	
C3	Utsunohira	Kiel	F1.27.1.94	A	n.a.	$y = 0.0006(1 + 0.0007)^x$ $R^2 = 0.996$	0.0007	1.00	
C4	Utsunohira	Kiel	F1.27.1.95	A	n.a.	$y = 0.0006(1 + 0.0007)^x$ $R^2 = 0.996$	0.0007	1.00	

Results

Periods around ~ 14 and 29 days are the most frequent with very high significance possibly proving the effects tides and lunar month (see Fig. 8). Besides these short-term cycles, naturally grown specimens show also intermediate term periods of ~ 60 to 85 days (Gamonts Sesoko) and long-term period of 213.6 days (Agamont Kekaa Point). As expected, the laboratory-cultured gamonts show different cyclicity patterns, as those seen in naturally grown foraminifera. Therefore they can be used to validate that these short-term cycles of natural grown specimens are environmentally induced.

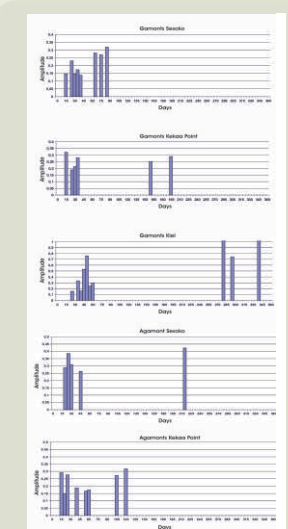


Fig. 8 Histograms of the most significant periods of the naturally grown gamonts and agamonts of Kekaa Point and Sesoko-Jima and of laboratory cultured gamonts from University of Kiel.

Conclusion

Larger benthic foraminifera record short to long-term oscillation during their chamber formation expressed as chamber size variation, which are affected by lunar oscillations. The approach of simulating complex environmental factors of natural marine habitats should be closely revised. Serendipity of very acute developed technologies support this view and create severe complications for further analysis using cultured specimens. Therefore, the validity of many geochemical analyses and environmental proxies applied on cultivated foraminifera may be badly affected.

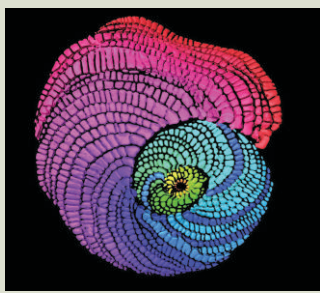


Fig. 9 complete 3D segmentation of a *Heterostegina depressa* agamont (B33) from Kekaa Point, Hawaii.

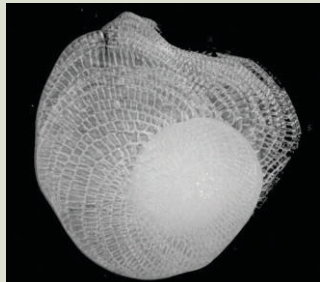


Fig. 10 the radiograph slices obtained by MicroCT analysis can also be used to reconstruct the foraminifer's test surface.

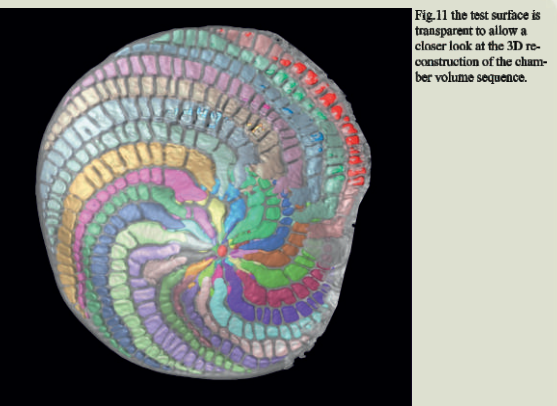


Fig. 11 the test surface is transparent to allow a closer look at the 3D reconstruction of the chamber volume sequence.

Briguglio, A., Wigger, J., Wölfling, E., Hohenegger, J., in press. Changing investigation perspectives: methods and applications of computed tomography on Larger Benthic Foraminifera. In: H. Kikano and J. Bernhard (Eds.), Experimental Approaches in Foraminifera: Collection, Maintenance and Experiments. Springer book, Environmental Science Series.

Perrillat-Cafardell, C., 2012. Multispiral growth in Nummulites: Paleobiological implications. Marine Micropaleontology 96-97. 105-122.

Hohenegger, J., 2011. Large Foraminifera: Greenhouse Constructions and Gardeners in the Oceanic Microcosm. The Kagoshima University Museum, Kagoshima, Japan. p. 85.

Hohenegger, J., Briguglio, A., Eder, W., in press. The natural laboratory of symbiotic bearing benthic foraminifera: Studying individual growth and population dynamics under natural conditions. In: H. Kikano and J. Bernhard (Eds.) Experimental Approaches in Foraminifera: Collection, Maintenance and Experiments. Springer book, Environmental Science Series.

Röttger, R., 1994. Untersuchungen zum Entwicklungsgang reiner Nummulitiden: *Heterostegina depressa*, *Nummulites venustus* und *Cyclonina carpenteri*. PhD-Thesis, Christian-Albrechts-Universität Kiel.